Developmental Biology 419 (2016) 298–310

Contents lists available at ScienceDirect

Developmental Biology

journal homepage: www.elsevier.com/locate/developmentalbiology

Original research article

Patterning of papillae on the mouse tongue: A system for the quantitative assessment of planar cell polarity signaling

Yanshu Wang [a,b], John Williams [a,b], Amir Rattner [a], Shu Wu [c,d], Alexander G. Bassuk [c,d], Andre M. Goffinet [e], Jeremy Nathans [a,b,f,g,*]

[a] Department of Molecular Biology and Genetics, Johns Hopkins University School of Medicine, Baltimore, MD, USA
[b] Howard Hughes Medical Institute, Johns Hopkins University School of Medicine, Baltimore, MD, USA
[c] Department of Neurology, University of Iowa, Roy J. and Lucille A. Carver College of Medicine, Iowa City, IA, USA
[d] Department of Pediatrics, University of Iowa, Roy J. and Lucille A. Carver College of Medicine, Iowa City, IA, USA
[e] Institute of Neuroscience, University of Louvain Medical School and WELBIO, B1200 Brussels, Belgium
[f] Department of Neuroscience, Johns Hopkins University School of Medicine, Baltimore, MD, USA
[g] Department of Ophthalmology, Johns Hopkins University School of Medicine, Baltimore, MD, USA

ARTICLE INFO

Article history:
Received 14 July 2016
Received in revised form
3 September 2016
Accepted 3 September 2016
Available online 6 September 2016

Keywords:
Planar cell polarity
Epithelial polarity
Papillae
Patterning

ABSTRACT

The dorsal surface of the mouse tongue is covered by ~7000 papillae, asymmetric epithelial protrusions that are precisely oriented to create a stereotyped macroscopic pattern. Within the context of this large-scale pattern, neighboring papillae exhibit a high degree of local order that minimizes the differences in their orientations. We show here that the orientations of lingual papillae are under the control of the core planar cell polarity (PCP) genes *Vangl1*, *Vangl2*, and *Celsr1*. Using *K14-Cre* and *Nkx2.5-Cre* to induce conditional knockout of *Vangl1* and/or *Vangl2* in the tongue epithelium, we observe more severe disruptions to local order among papillae with inactivation of larger numbers of *Vangl* genes, a greater role for *Vangl2* than *Vangl1*, and a more severe phenotype with the *Vangl2 Looptail* (*Lp*) allele than the *Vangl2* null allele, consistent with a dominant negative mode of action of the $Vangl2^{Lp}$ allele. Interestingly, $Celsr1^{-/-}$ tongues show disruption of both local and global order, with many papillae in the anterior tongue showing a reversed orientation. To quantify each of these phenotypes, we have developed and applied three procedures for sampling the orientations of papillae and assessing the degree of order on different spatial scales. The experiments reported here establish the dorsal surface of the mouse tongue as a favorable system for studying PCP control of epithelial patterning.

1. Introduction

The epithelial surfaces of many metazoa exhibit complex sub-cellular, cellular, and/or multi-cellular structures that are arranged in precise and spatially asymmetric patterns. Well known examples of such structures include (1) hairs and bristles on the insect wing and cuticle, (2) scales, feathers, and hair on the skin of reptiles, birds, and mammals, respectively, and (3) the motile cilia that line the trachea, lateral ventricles, and fallopian tubes. These structures exhibit spatial order within the plane of the epithelium and each of them has an axis of asymmetry that is oriented relative to the global asymmetry of the body axes or other large-scale body structures.

The polarity of cellular structure within the plane of an epithelium, referred to as planar cell polarity (PCP), has been analyzed extensively in *Drosophila*, zebrafish, *Xenopus*, and mice (Adler et al., 2002; Goodrich and Strutt, 2011). Pioneering genetic studies in *Drosophila* revealed two inter-related systems – the *Van Gogh* (*Vang*)/*Frizzled* (*Fz*)/*Starry night* (*Stan*) and the *Fat/Dachsous* systems – that utilize cell-surface proteins to transmit polarity information between neighboring cells within an epithelium (Lawrence et al., 2007; Matis and Axelrod, 2013). Each of these "core" PCP genes has multiple homologues in vertebrate genomes. In mice, analyses of the phenotypes produced by conventional and/or conditional knockout of core PCP genes, either singly or in combination, have revealed multiple epithelial structures that utilize PCP signaling. These include hair follicles (*Celsr1*, *Fz6*, *Vangl2*; Guo et al., 2004; Wang et al., 2006a; Devenport and Fuchs, 2008; Ravni et al., 2009; Wang et al., 2010), inner ear sensory hair cells (*Celsr1*, *Dsh*, *Fz3*, *Fz6*, *Vangl2*; Curtin et al., 2003; Montcouquiol et al., 2003; Wang et al., 2005; Wang et al., 2006b), and motile cilia (*Celsr1-3*, *Dsh*, *Vangl1*; Tissir et al., 2010; Vladar et al., 2012; Boutin et al., 2014; Ohata et al., 2014; Shi et al., 2014).

* Corresponding author at: Department of Molecular Biology and Genetics, Johns Hopkins University School of Medicine, Baltimore, MD, USA.
E-mail address: jnathans@jhmi.edu (J. Nathans).

http://dx.doi.org/10.1016/j.ydbio.2016.09.004
0012-1606/

The polarized epithelial protrusions that cover the dorsal surface of the tongue, referred to here as lingual papillae (LP), represent the most recent addition to this list. Hua et al. (2014) demonstrated that the orientations of LP are regulated by PCP genes *Fz3* and *Fz6*. Eliminating *Fz3* selectively in the epidermis with a *Keratin14-Cre* transgene ($Fz3^{CKO/-}$;*K14-Cre*; *CKO*, conditional knockout) or eliminating *Fz6* constitutively ($Fz6^{-/-}$) did not alter the LP pattern, but combining both of these genetic alterations ($Fz3^{CKO/-}$;$Fz6^{-/-}$;*K14-Cre*) produced a mild disruption in the local order of LP, primarily in the anterior of the tongue.

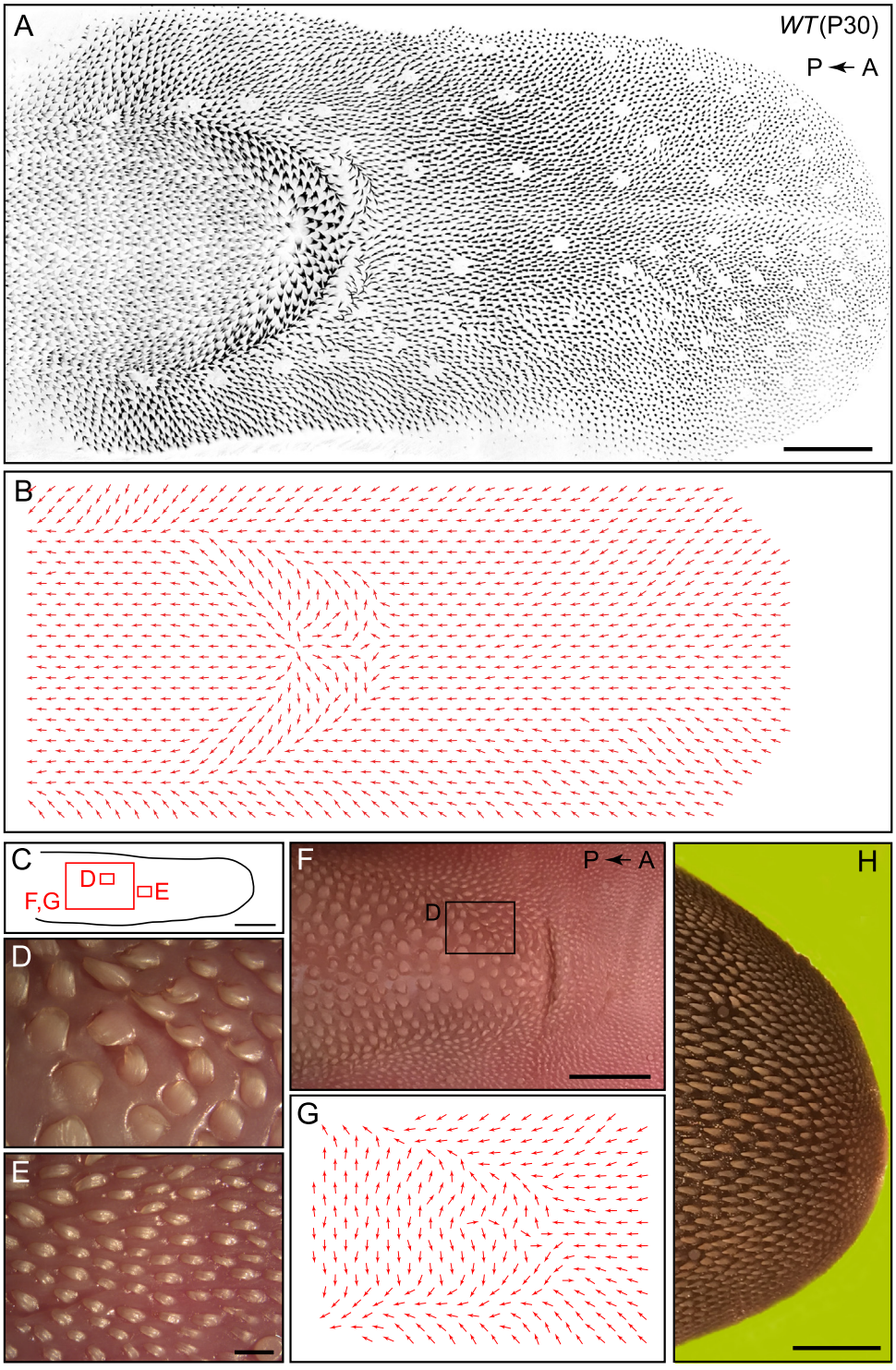

Fig. 1. Similar patterns of LP on the dorsal surface of mouse and bovine tongues. (A) *WT* P30 mouse tongue. Anterior is to the right. The flower region is centered ~65% of the distance from anterior to posterior. Small white circular regions correspond to fungiform papillae (taste buds). A small indentation is characteristically seen at the anterior border of the flower region. A, anterior; P, posterior. (B) Manual scoring of the LP vector field in (A) using a regular grid of vectors (red arrows) and visually interpolating the mean orientation of LP in the immediate neighborhood of each vector. (C–H) Dorsal surface patterns of LP on the adult bovine tongue. In all images, anterior is to the right. (C) Locations of panels (D-G). (D) LP in the bovine equivalent of the flower region. (E) LP anterior to the flower region. (F) The flower region (leftmost 70% of the image) and the adjacent anterior region (rightmost 30% of the image). As in the mouse tongue, the two territories are separated by a transverse indentation. (G) Manual scoring of the LP vector field in (F). (H) Anterior tip of a bovine tongue showing LP oriented from anterior to posterior. Scale bars: (A), 1 mm; (C), 5 cm; (F), 2 cm; (H), 1 cm.

In the present study, we have asked whether other PCP genes (*Vangl1*, *Vangl2*, and *Celsr1*) play a role in LP patterning and whether genetic disruptions in these PCP gene can produce defects in LP orientation that are more severe or extensive than the relatively mild phenotype observed in *Fz3*$^{CKO/-}$;*Fz6*$^{-/-}$;*K14-Cre* mice. We have also explored the cross-species conservation of the LP pattern. Finally, we have optimized the tongue preparation and imaging methodology and developed algorithms for quantitative analyses of LP phenotypes based on different strategies for sampling LP orientations. This work demonstrates that the dorsal surface of the tongue is a technically favorable tissue in which to study macroscopic epithelial patterning in general and PCP-dependent patterning in particular.

2. Results

2.1. The pattern of mouse LP and the conservation of this pattern across species

In previous work (Hua et al., 2014), LP on the dorsal surface of the tongue were visualized in whole mount preparations by genetic labeling with *Keratin* (*K*)*17-GFP* (Bianchi et al., 2005) or by systemic administration of the fixable dye AM4-65. More recently, we observed that the tongue epithelium of mice that are >2–3 weeks of age exhibit endogenous fluorescence that can be used to visualize LP. Confocal Z-stacked images were obtained from flattened and immersion fixed tongues at postnatal day (P)30 and were then stitched together to produce a single 6 mm $\times$ 10 mm image. In the figures, image intensities have been inverted, rendered in gray scale, and contrast enhanced so that fluorescent pixels appear dark gray or black.

The overall arrangement of papillae on the surface of the mouse tongue was described by Kutuzov and Sicher (1953) and is confirmed and extended by the confocal imaging described here. In wild type (*WT*) mice, the dorsal surface of the tongue is covered by $\sim$7000 LP that are organized into a stereotyped pattern in which LP on the anterior $\sim$60% and the posterior $\sim$30% of the tongue are oriented posteriorly, and LP along the lateral sides of the tongue are oriented in a posterior/medial direction (Fig. 1A and B). The most striking feature of this pattern is a group of several hundred LP radiating from a point that is centered at the midline between 60% and 70% of the distance from the tongue anterior. We refer to this pattern element as the “flower region” because of its similarity to the radially oriented petals of a flower. The only two regions with local discontinuities in LP orientation are (1) the center of the flower region, where LP orientations cover the full 360 degree range, and (2) the border between the anterior flower region, with LP pointing anteriorly, and the adjacent anterior region of the tongue, with LP pointing posteriorly. As seen in Fig. 1A and B, many LP straddling the flower region/anterior region border are oriented in a medio-lateral direction, leaving only a single point of sharp discontinuity in orientation at the midline. In all other regions, LP exhibit spatially graded changes in orientation that reduce orientation differences between neighbors. We note that Kutuzov and Sicher (1953) distinguished among surface papillae based on their size and shape, referring to the anterior papillae as conical, the posterior papillae as filiform, and the papillae in the flower region as giant.

The tongues of many mammalian species have LP, an adaptation of epithelial structure that is presumably advantageous for grooming and feeding (Doran, 1975; Iwasaki, 2002). To explore the evolutionary conservation of LP patterning, we examined rat and cow tongues. As described by Kutuzov and Sicher (1951, 1953), we observed that rats exhibit a pattern of LP orientations nearly identical to that in mice (data not shown). Remarkably, cows also have a similar pattern with posteriorly directed LP over the anterior $\sim$60% of the tongue and an elongated flower region in which the center is extended along the midline with LP radiating laterally (Fig. 1C–H). The similarity between mouse and cow LP patterns is especially striking because the last common ancestor of these species is estimated to have lived >50 Myr ago (Bininda-Emonds et al., 2007). An adult cow tongue is $\sim 30\times$ larger in linear dimensions than an adult mouse tongue (30 cm vs. 1 cm length) and the largest bovine LP are approximately half the width of the adult mouse tongue ($\sim$2 mm). These size comparisons indicate that the developmental mechanisms controlling LP pattern can accommodate differences of several orders of magnitude in the number of cells per LP.

2.2. Vangl1 and Vangl2 deletions mediated by K14-Cre

As noted in the Introduction, *Fz3*$^{CKO/-}$;*Fz6*$^{-/-}$;*K14-Cre* tongues exhibit a mild LP misorientation phenotype that is most apparent on the anterior of the tongue. In light of the mutual redundancy of these two proteins in the tongue, a possible explanation for the mildness of the *Fz3*$^{CKO/-}$;*Fz6*$^{-/-}$;*K14-Cre* phenotype is that one or more of the eight other mammalian *Frizzled* genes might also be expressed in the tongue and provide partially redundant function. To circumvent the difficulties inherent in genetic analyses with such a large gene family, we focused instead on *Vangl1* and *Vangl2*, which comprise the smallest family of core PCP genes in mammals. In earlier work, mutations in one or both of the two *Vangl* genes had been found to produce sensory hair cell misorientation in the inner ear, hair follicle misorientation in the skin, motile cilia misorientation in the trachea, and craniorachischisis (Murdoch et al., 2001; Montcouquiol et al., 2003; Devenport and Fuchs, 2008; Torban et al., 2008; Wang et al., 2010; Chang et al., 2016).

As constitutive inactivation of *Vangl2* is incompatible with postnatal life (Yin et al., 2012), our experiments utilized conditional inactivation of *Vangl1* and/or *Vangl2* with either an epithelial-specific *Cre* (*K14-Cre*; Dassule et al., 2000) or a heart- and tongue-specific *Cre* (*Nkx2.5-Cre*; Moses et al., 2001). For both *Cre* drivers, *Cre* activity in the developing tongue was assessed at daily intervals between E11 and E14 using a reporter consisting of a *CAG promoter/loxP-stop-loxP/tdTomato* knock-in at the *Hprt* locus (*Hprt-LSL-tdT*; Wu et al., 2014; Fig. S1). *Nkx2.5-Cre*-mediated recombination begins in the tongue primordium at $\sim$E11 and *K14-Cre*-mediated recombination begins $\sim$1 day later. By E14, both drivers produce essentially complete recombination throughout the tongue epithelium. As seen in the E14 cross-sections in Fig. S1 (panels C and F), *Nkx2.5-Cre* is expressed in both the tongue epithelium and the underlying musculature, while *K14-Cre* is expressed only in the epithelium.

Fig. 2 shows representative P30 tongue flat mounts from a series of genotypes that differ with respect to the number of mutant *Vangl1* and/or *Vangl2* alleles, and in which recombination of one or both *CKO* alleles is mediated by *K14-Cre*. Comparing the *WT* control (*Vangl1*$^{CKO/+}$;*Vangl2*$^{CKO/+}$; Fig. 2A) and the double *KO* (*Vangl1*$^{CKO/-}$;*Vangl2*$^{CKO/-}$;*K14-Cre*; Fig. 2E) shows that conversion of both Vangl genes from heterozygous to homozygous null starting at $\sim$E12 leads to (1) severe disorganization in the posterior flower region, (2) milder disorganization in the anterior flower region, and (3) a gradient of disorganization in the anterior region, with LP show the greatest disorganization toward the anterior of the tongue. All *Vangl1* and/or *Vangl2* mutant or conditional mutant combinations showed this pattern of LP disorganization, with the severity of the phenotype depending on the number of mutant alleles and the *Cre* driver.

Inactivation of *Vangl1* and *Vangl2* did not affect the size, shape, density, or location of LP. In particular, the division of LP patterns into flower and anterior regions, each with characteristic LP sizes

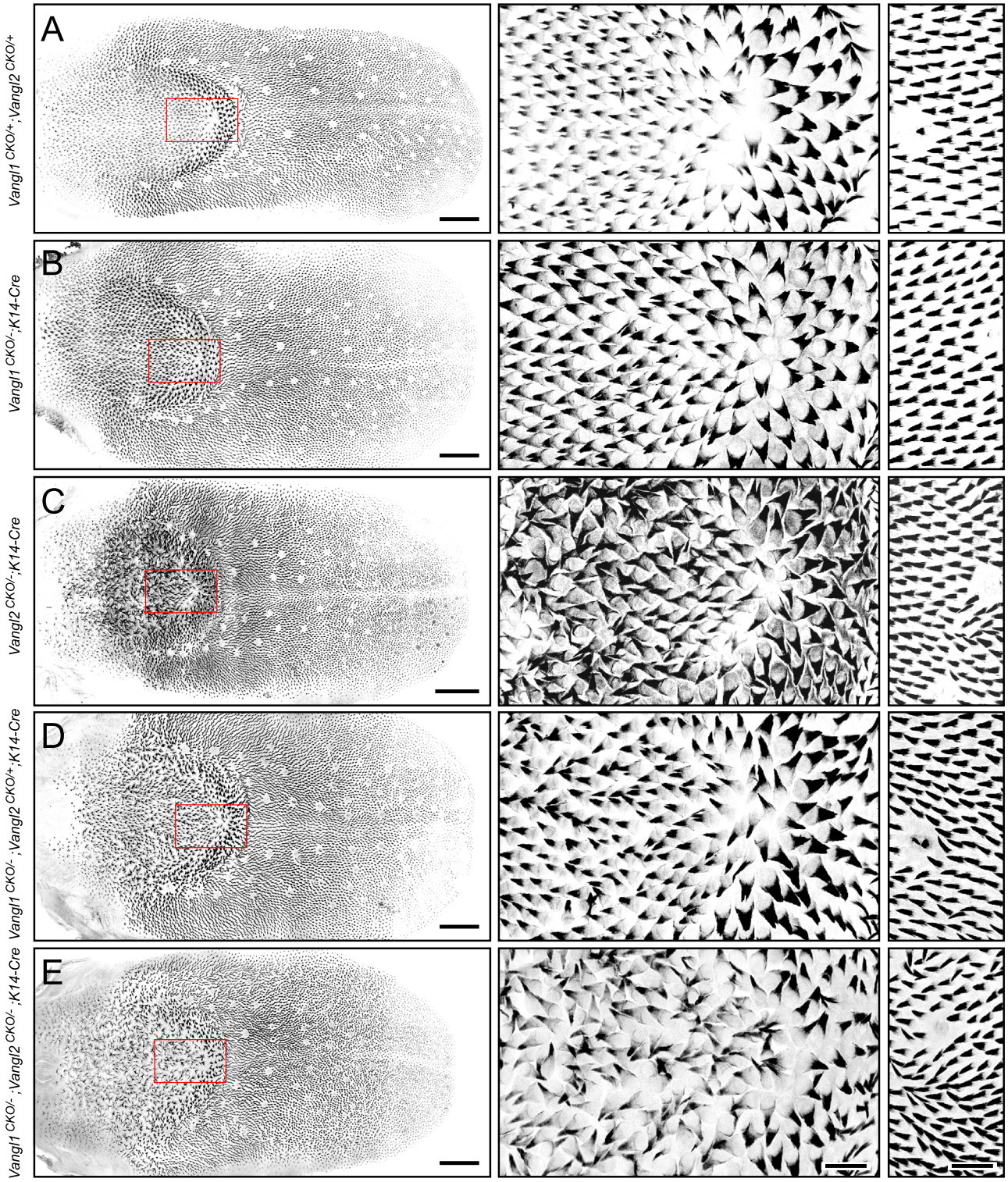

Fig. 2. Flat mounts of the dorsal surface of *K14-Cre* tongues at P30 show greater misorientation of LP with inactivation of greater numbers of *Vangl* genes. Stitched tongue images (left column), flower region (enlarged, center column; corresponding to the red boxed regions in the left column), and anterior region ~1 mm anterior to the anterior edge of the flower region (enlarged, right column). Genotypes correspond to *WT* (top row), inactivation of both *Vangl1* alleles (second row), inactivation of both *Vangl2* alleles (third row), inactivation of three alleles (one *Vangl2* allele remaining, fourth row), and inactivation of all four *Vangl* alleles (bottom row). Anterior is to the right. Scale bars: left column, 1 mm; center and right columns, 200 μm.

and shapes, was unaltered. The number and general distribution of fungiform papillae (taste buds) was also unchanged. As observed with PCP phenotypes in the hair follicle system (Wang et al., 2006a, 2010), the phenotypes observed here are limited to defects in orientation.

Inactivation of *Vangl1* alone (Fig. 2B) leads to subtle defects in LP orientation, as seen in the posterior flower region, whereas inactivation of *Vangl2* alone (Fig. 2C) leads to a more severe disorganization in the flower region and a modest disorganization in the anterior region. The greater role of *Vangl2* relative to *Vangl1* is

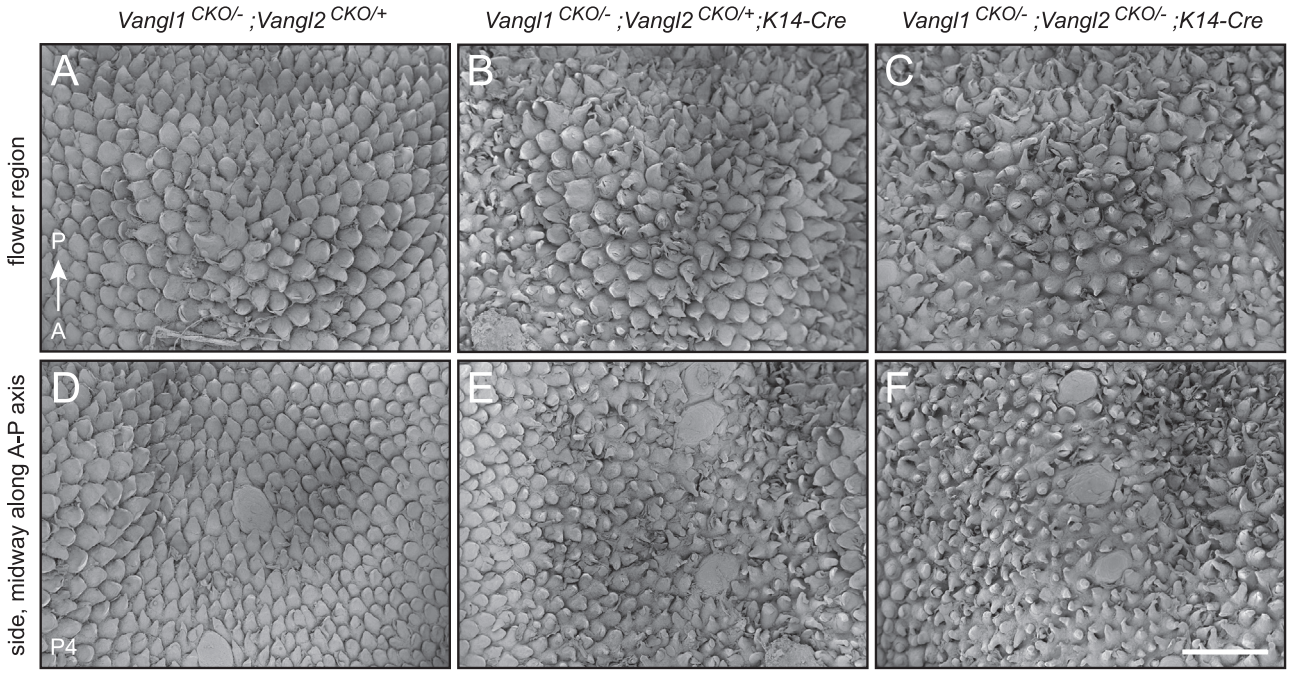

Fig. 3. Scanning electron micrographs of the dorsal surface of *K14-Cre* tongues at P4 show greater misorientation of LP with inactivation of greater numbers of *Vangl* genes. (A–C) The flower region and (D–F) the anterior region at ~50% of the distance from the anterior end of the tongue and to the side of the midline. In all images, anterior is toward the bottom of the image as indicated by the A–P arrow in (A). The larger flat structures are fungiform papillae (taste buds); the smaller structures are LP. Genotypes range from inactivation of only one allele of *Vangl1* (A and D) to inactivation of all four *Vangl* alleles (C and F). Scale bar, 200 μm.

also seen in the comparison between *Vang12*$^{CKO/-}$*;K14-Cre* (Fig. 2C) and *Vangl1*$^{CKO/-}$*;Vangl2*$^{CKO/+}$*;K14-Cre* (Fig. 2D), which shows that, among the four *Vangl* alleles, the presence of only a single *WT Vangl2* allele leads to a more *WT*-like phenotype than does the presence of two *WT Vangl1* alleles. The trend of greater phenotypic severity with a greater number of mutant *Vangl* alleles was observed at P4 by scanning electron microscopy in both flower and anterior regions (Fig. 3).

To assess the extent to which the correlation between *Vangl* genotype and phenotypic severity generalizes beyond the LP system, hair follicles on the tail were imaged for WT, three allele inactivation (*Vangl1*$^{CKO/-}$*;Vangl2*$^{CKO/+}$*;K14-Cre* and *Vangl1*$^{CKO/+}$*; Vangl2*$^{CKO/-}$*;K14-Cre*), and four allele inactivation (*Vangl1*$^{CKO/-}$*; Vangl2*$^{CKO/-}$*;K14-Cre*) at P4 using follicle-specific fluorescent labeling with *K17-GFP* (Fig. S2). In agreement with an earlier analysis of hair follicles on the back (Chang et al., 2016), inactivation of *Vangl2* is associated with a more severe hair follicle misorientation phenotype than inactivation of *Vangl1*, with the same trend of increasing severity of misorientation as was observed among LP.

As noted above, LP may confer a selective advantage in the contexts of eating and grooming (Doran, 1975; Iwasaki, 2002). To roughly assess the contribution of LP orientation to overall health, mice with various combinations of *Vangl1*, *Vangl2*, and *K14-Cre* alleles were weighed at three-day intervals from P6 to P21 (N = 116 mice; Fig. S3; Table S1). At all six time points examined, *Vangl1*$^{CKO/-}$*;Vangl2*$^{CKO/-}$*;K14-Cre* mice (N = 33) were approximately 10% smaller than their *Vangl1*$^{CKO/-}$*;Vangl2*$^{CKO/+}$*;K14-Cre* (N = 32) and *WT* (N = 18) littermates ($P < 0.0002$ for both comparisons at every time point), whereas the latter two genotypes were not significantly different from each other at any time point (P = 0.08–0.86). Among littermates lacking *K14-Cre* [*Vangl1*$^{+/-}$*;Vangl2*$^{+/-}$ (N = 8), *Vangl1*$^{+/-}$ (N = 9), *Vangl2*$^{+/-}$ (N = 16), and *WT* (N = 18)], the mean weights of *Vangl1*$^{+/-}$*;Vangl2*$^{+/-}$ mice were lower at all time points relative to the other three genotypes, with some P-values above and others below 0.05. As *Vangl1* and *Vangl2* are widely expressed throughout development, it is not clear which anatomic or functional perturbations are responsible for the weight phenotype among mice that are heterozygous for these genes in all tissues and at all developmental times. By contrast, the limited domain of *K14-Cre* expression suggests that the low weight phenotype of *Vangl1*$^{CKO/-}$*;Vangl2*$^{CKO/-}$*;K14-Cre* mice might be due to an effect of LP orientation on suckling efficiency.

2.3. Quantitative comparisons among Vangl1 and Vangl2 deletions mediated by Nkx2.5-Cre

Although the *Vangl1*$^{CKO/-}$*;Vangl2*$^{CKO/-}$*;K14-Cre* tongue exhibits severe and widespread LP misorientation, the many LP with approximately correct orientations suggest that the observed phenotype might constitute only a partial loss of PCP signaling. With the goal of obtaining a *Vangl1/Vangl2* series with a more severe LP phenotype, we explored the use of *Nkx2.5-Cre* (Fig. 4), which – as noted above – is expressed in the tongue epithelium one day earlier than *K14-Cre* (Fig. S1). By visual inspection, *Nkx2.5-Cre* consistently produces a more severe LP orientation phenotype than *K14-Cre*, as seen, for example, by comparing *Vangl1*$^{CKO/-}$*; Vangl2*$^{CKO/+}$*;K14-Cre* (Fig. 2D) vs. *Vangl1*$^{CKO/-}$*;Vangl2*$^{CKO/+}$*;Nkx2.5-Cre* (Fig. 4B) and *Vangl1*$^{CKO/-}$*;Vangl2*$^{CKO/-}$*;K14-Cre* (Fig. 2E) vs. *Vangl1*$^{CKO/-}$*;Vangl2*$^{CKO/-}$*;Nkx2.5-Cre* (Fig. 4D). It is possible that the greater severity of the LP misorientation phenotype in the *Nkx2.5-Cre* series relative to the *K14-Cre* series reflects expression of *Nkx2.5-Cre* (and, therefore deletion of *Vangl* genes) in both mesenchymal and epithelial cells in the tongue, compared to the epithelial-only expression pattern of *K14-Cre* (Fig. S1C and F). However, we think that this explanation is unlikely as Vangl proteins are readily detectable in epithelial cells but undetectable in mesenchymal cells in the prenatal tongue by immunostaining (data not shown).

As qualitative assessments of PCP phenotypes are of limited value, we have explored three strategies for sampling and quantifying LP orientations. In the first method, referred to as the “circle method”, two sets of sixteen 400 μm diameter circles, arranged in 4×4 squares, were laid over the tongue image, with one 4×4 square over the posterior part of the flower region and the other

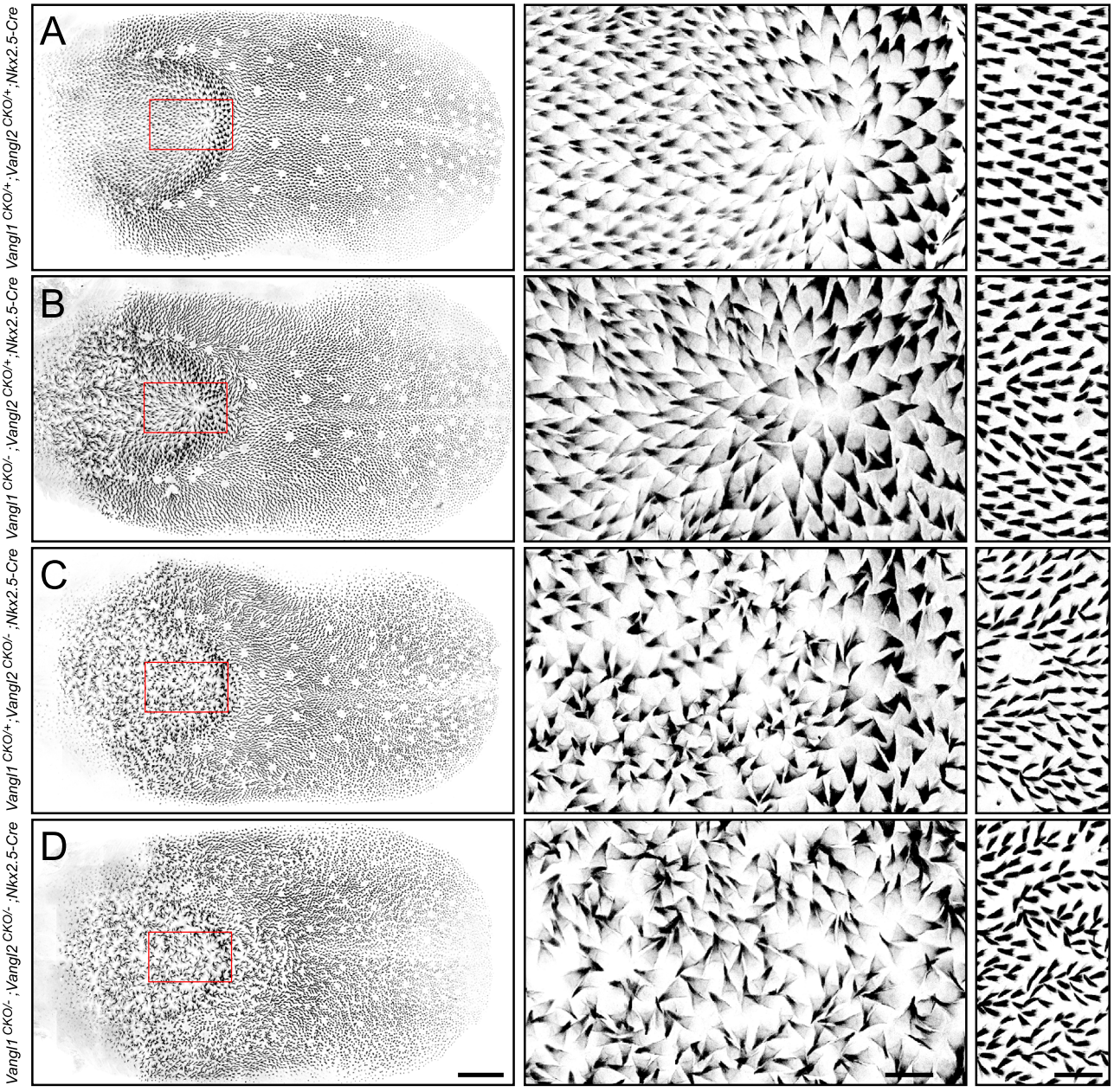

Fig. 4. Flat mounts of the dorsal surface of *Nkx2.5-Cre* tongues at P30 show greater misorientation of LP with inactivation of greater numbers of *Vangl* genes. Stitched tongue images (left column), flower region (enlarged, center column; corresponding to the red boxed regions in the left column), and anterior region ~1 mm anterior to the anterior edge of the flower region (enlarged, right column). Genotypes correspond to inactivation of two alleles (heterozygosity for both *Vangl1* and *Vangl2*; top row), inactivation of three alleles (one *Vangl2* allele remaining, second row; or one *Vangl1* allele remaining, third row), and inactivation of all four *Vangl* alleles (bottom row). Anterior is to the right. Scale bars: left column, 1 mm; center and right columns, 200 μm.

4×4 square over the anterior region as shown in Fig. 5A. These two locations were chosen because they represent one territory with a high degree of LP disorganization (the posterior territory) and another with a modest degree of LP disorganization (the anterior territory). The orientations of the ~30 LP within each circle were determined manually, and then the circular standard deviation was calculated for the set of vector orientations contained within each circle (Fig. 5B). Using the circle method to quantify LP from *WT* and from three *Vangl1/Vangl2/Nkx2.5-Cre* genotypes with inactivation of either three or four *Vangl* genes (two tongues per genotype), we observe highly significant differences between *WT* and all mutants in both the anterior and posterior territories, between $Vangl1^{CKO/-}$;$Vangl2^{CKO/+}$;*Nkx2.5-Cre* and $Vangl1^{CKO/+}$;$Vangl2^{CKO/-}$;*Nkx2.5-Cre* in the posterior territory, and between $Vangl1^{CKO/+}$;$Vangl2^{CKO/-}$;*Nkx2.5-Cre* and $Vangl1^{CKO/-}$;$Vangl2^{CKO/-}$;*Nkx2.5-Cre* in the anterior territory (Fig. 5C).

In the second method of sampling and quantifying LP orientation, referred to as the "line method", we have (1) scored the orientations of LP that intersect a series of five horizontal lines placed over the anterior territory (at the same location as the anterior 4×4 set of circles in the circle method; Fig. 6A), and then (2) calculated the average angular difference between nearest neighbor LP for each of the ~40 LP per line (Fig. 6B). Inherent in this protocol is an under-sampling of LP that are oriented parallel to the line compared to LP that are oriented perpendicular to the line, as illustrated in Fig. 6C. This differential sampling can be eliminated by modifying the protocol to score intersections between the horizontal line and a circular territory that is centered on each LP and that has a diameter equal to the length of the LP (Fig. 6C).

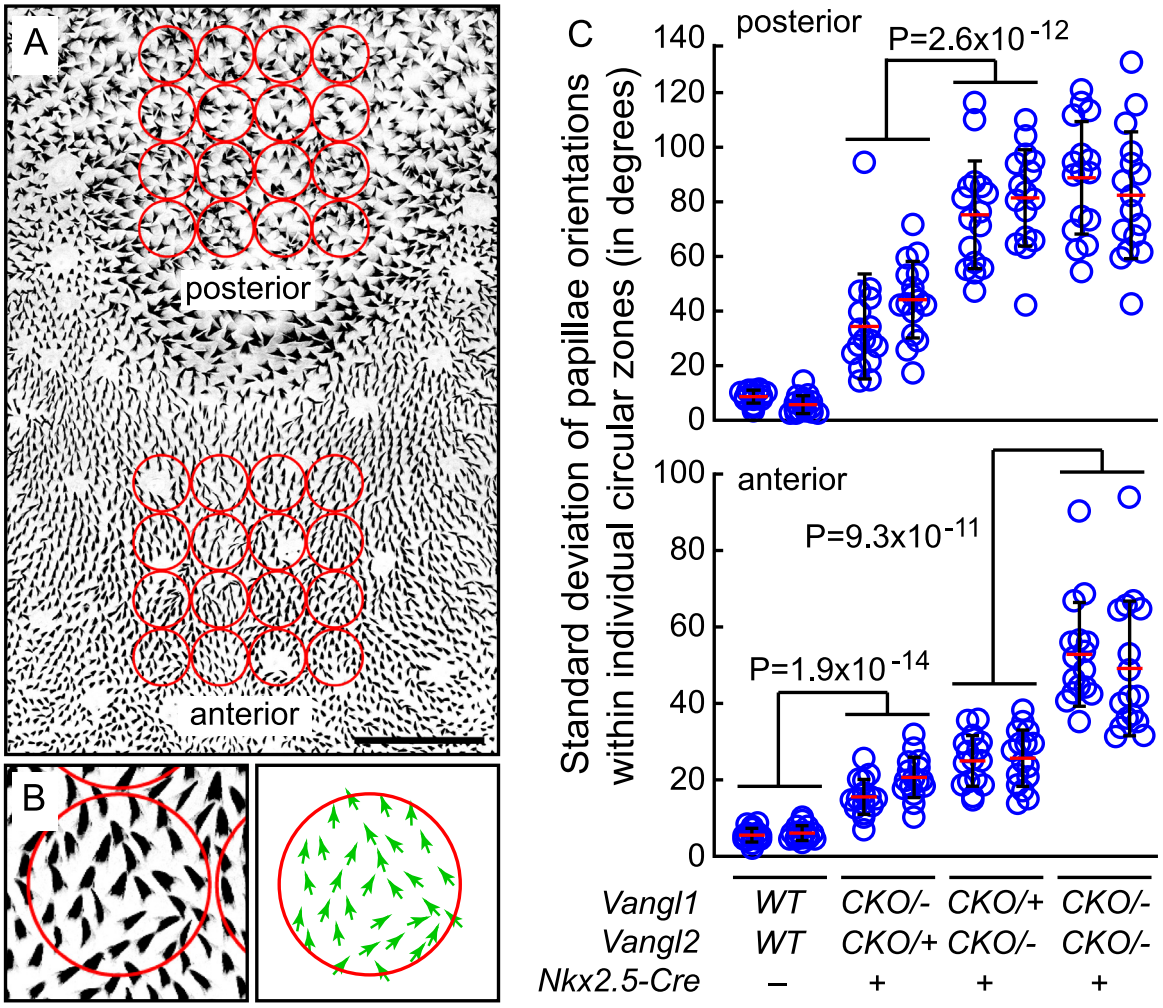

Fig. 5. The circle method for quantifying local LP orientation applied to *Nkx2.5-Cre* tongues with inactivation of different numbers of *Vangl* genes. (A) The standard placement of the anterior and posterior sets of $4 \times 4 = 16$ circles. (D) Example showing LP within a circle (left) and manual scoring of their orientations (right). (C) The circular standard deviation of LP orientations within 16 circular zones from the posterior flower region (upper panel) and within 16 circular zones from the anterior region (lower panel) from each of two tongues for the indicated genotypes, which correspond to *WT*, three allele inactivation (one *WT Vangl2* allele remaining or one *WT Vangl1* allele remaining), and four allele inactivation, all mediated by *Nkx2.5-Cre*. Scale bar in (B): 1 mm.

The line method was used to assess LP orientations in the same set of *Vangl1;Vangl2;Nkx2.5-Cre* tongues analyzed with the circle method (Fig. 6D). The results are in close agreement with data from the circle method that was obtained for the same anterior region: statistically significant differences were found between *WT* and all three *Vangl* mutants, between genotypes with inactivation of three vs. four *Vangl* genes, but not between the two genotypes with inactivation of three *Vangl* genes (*Vangl1*$^{CKO/-}$;*Vangl2*$^{CKO/+}$;*Nkx2.5-Cre* vs. *Vangl1*$^{CKO/+}$;*Vangl2*$^{CKO/-}$;*Nkx2.5-Cre*). Using the line method, a quantitative comparison between the *K14-Cre* and *Nkx2.5-Cre* series of tongues (*Vangl1*$^{CKO/-}$;*Vangl2*$^{CKO/+}$;*K14-Cre* vs. *Vangl1*$^{CKO/-}$;*Vangl2*$^{CKO/+}$;*Nkx2.5-Cre* and *Vangl1*$^{CKO/-}$;*Vangl2*$^{CKO/-}$;*K14-Cre* vs. *Vangl1*$^{CKO/-}$;*Vangl2*$^{CKO/-}$;*Nkx2.5-Cre*) confirmed the visual impression that the *K14-Cre* series exhibits a milder misorientation phenotype than does the *Nkx2.5-Cre* series (Fig. S4).

The circle and line methods assess local order/disorder but they do not make fine distinctions between different patterns of angular deviation. To illustrate this point, Fig. 6E shows four linear arrangements of sixteen vectors in which the mean angular deviation between nearest neighbors is six degrees, equivalent to 90 degrees total deviation for the fifteen nearest neighbor pairs. The line method produces the same score for all four arrangements, and analogous arrangements of vectors in two dimensions yield equivalent scores with the circle method. Thus, distinguishing between these four vector arrangements requires a different LP sampling strategy.

2.4. Comparison of Vangl2 null and Looptail alleles

To further test the utility of tongue LP orientation as a quantitative system for evaluating PCP signaling, we compared the *Vangl2* null allele and the *Vangl2 Looptail* (*Lp*) allele, an amino acid substitution mutation that functions as a dominant negative in the context of inner ear and neural tube closure phenotypes (Yin et al., 2012). Since *Vangl2*$^{Lp/Lp}$ mice die at birth with craniorachischisis, we have studied the *Lp* allele in the context of conditional inactivation of *Vangl1* and/or *Vangl2* using *K14-Cre*. As judged by visual inspection (Fig. 7A) and as quantified by the line and circle methods (Fig. 7C and D), *Vangl1*$^{+/-}$;*Vangl2*$^{+/Lp}$ tongues show a substantially greater severity of LP misorientation than *Vangl1*$^{+/-}$;*Vangl2*$^{+/-}$ tongues, especially in the posterior region, consistent with a model in which the *Lp* allele interferes with *Vangl* function. A more modest difference in phenotypic severity is seen in comparing *Vangl2*$^{CKO/-}$;*K14-Cre* vs. *Vangl2*$^{CKO/Lp}$;*K14-Cre* tongues (compare Figs. 2C and 7B; quantification in Fig. 7C). Interestingly, the comparison of *Vangl2* null vs. *Lp* alleles shows a smaller difference in phenotypic severity when all of the other *Vangl* genes are inactivated (*Vangl1*$^{CKO/-}$;*Vangl2*$^{CKO/-}$;*K14-Cre* vs. *Vangl1*$^{CKO/-}$;

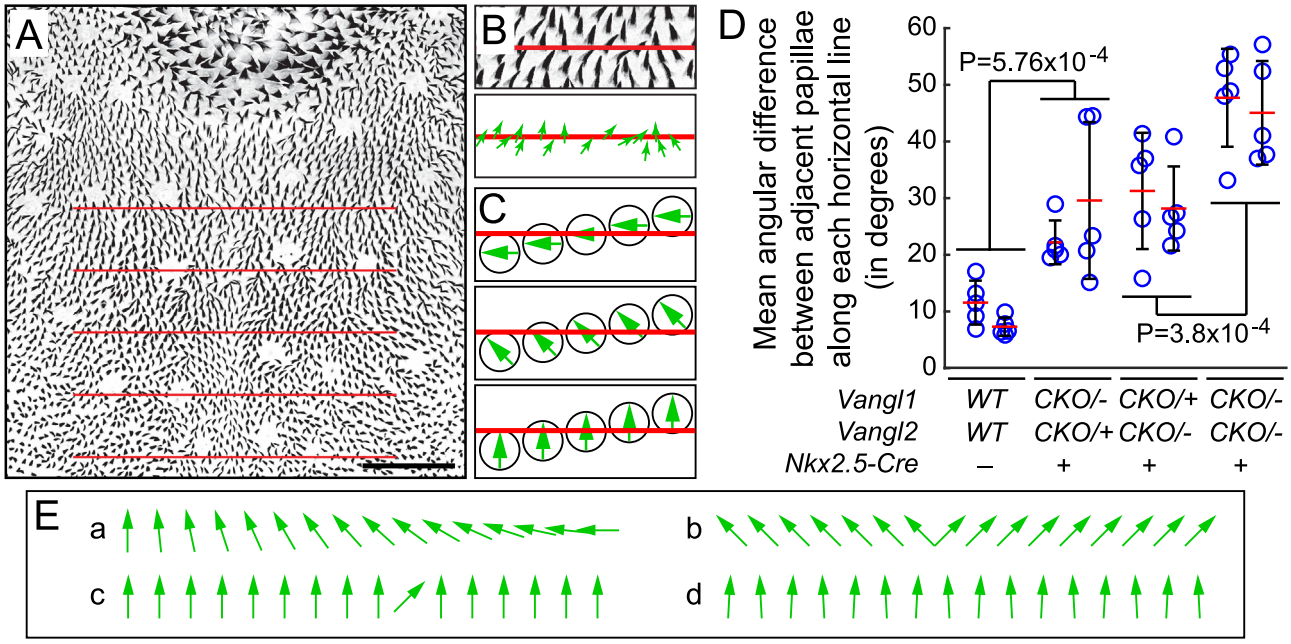

Fig. 6. The line method for quantifying local LP orientation applied to *Nkx2.5-Cre* tongues with inactivation of different numbers of *Vangl* genes. (A) The standard placement of the five horizontal lines within the anterior zone of LP. (B) Enlarged region from (A) with scoring of LP angles for those papillae that overlap the horizontal line (red). (C) Illustration of the points of overlap between papillae (shown schematically as green arrows), a circular territory centered on each papilla (black circle), and a horizontal red line, as a function of papilla angle and location of the midpoint of the papilla. Papillae oriented parallel to the line (top image) do not overlap the line unless the midpoint of the papillae is close to the line. (D) Mean angular differences between adjacent papillae along each of five horizontal lines from each of two tongues for the indicated genotypes. (E) Four linear arrangements of sixteen vectors with total angular deviations between the fifteen pairs of nearest neighbors of 90 degrees. In (a) each vector was rotated six degrees counter-clockwise relative to its left neighbor; in (b) left and right sets of vectors were rotated 45 degrees counterclockwise or clockwise, respectively; in (c) one vector was rotated 45 degrees, and in (d) the vectors were rotated three degrees counter-clockwise or clockwise in alternation. Scale bar in (B): 1 mm.

Vangl2$^{CKO/Lp}$;*K14-Cre*) or when all of the other *Vangl* alleles are present (*Vangl2*$^{+/-}$ vs. *Vangl2*$^{+/Lp}$). In the former case, there is a severe LP misorientation phenotype in both null and *Lp* genotypes (quantified in Fig. 7C), and in the latter case there is an LP pattern that is indistinguishable from *WT* (data not shown).

We can rationalize the differential severity of the *Vangl2 null* vs. *Lp* phenotypes described above by hypothesizing that the phenotypic consequences of the dominant negative action of the *Lp* allele are most evident when the total *Vangl* activity is marginally above a minimum threshold required for PCP signaling. This model predicts: (1) that there will be little or no phenotypic consequence of the dominant negative allele when the other three *Vangl* alleles have been eliminated and there is no *Vangl* activity, and (2) at the opposite extreme, when the other three *Vangl* alleles are present and total *Vangl* activity is substantially above the threshold there will be little or no phenotypic difference between dominant negative and null alleles since neither reduces the total *Vangl* activity below the threshold level. In the context of this model, we hypothesize that the presence of one *WT Vangl1* allele and one *WT Vangl2* allele produces a level of *Vangl* activity in the tongue that is marginally above the threshold for normal PCP signaling, which leads to a large phenotypic effect when the null allele is replaced by the *Lp* allele and the total *Vangl* activity level is reduced below that threshold.

2.5. The LP patterning phenotype produced by inactivation of Celsr1

To date, hair follicle misorientation phenotypes have been described for three classes of PCP genes: *Frizzled* (*Fz6*), *Vangl* (*Vangl1* and *Vangl2*), and *Celsr* (*Celsr1*). The work of Hua et al. (2014) and the experiments described above, show that *Frizzled* and *Vangl* also control LP orientation on the dorsal surface of the tongue. To determine whether *Celsr1* also plays a role in LP orientation, we examined flat mounts of *Celsr1*$^{-/-}$ and *Celsr1*$^{+/-}$, tongues at P30 (Fig. 8). Homozygous inactivation of *Celsr1* produces an LP misorientation phenotype. A similar analysis with *Prickle2*, one of four members of a gene family that codes for cytoplasmic adaptor proteins involved in PCP signaling (Deans et al., 2007; Sharp et al., 2016), showed no alterations in homozygous *Prickle2* mutant tongues (data not shown).

Celsr1$^{-/-}$ tongues show the same general features as *WT* tongues: a normal number and distribution of fungiform papillae, the presence of flower and anterior regions, and the same distinctive variation in LP morphology in different regions of the tongue. However, *Celsr1*$^{-/-}$ tongues show a distinctly different pattern of LP misorientation compared to that seen with the *Vangl1*;*Vangl2* series (Fig. 8A–D). While *Celsr1*$^{-/-}$ tongues exhibit a level of local variation in LP orientation that roughly matched the midpoint of the phenotypic range for LP misorientation in the *Vangl1*;*Vangl2* series (as determined by both the circle and line methods; Fig. 8E and F), many of the anterior LP on *Celsr1*$^{-/-}$ tongues exhibit global defects in orientation (Fig. 8B–D). The extent and location of the global misorientation was consistent across multiple tongues as can be seen from the vector maps of the anterior regions of three *Celsr1*$^{-/-}$ tongues (Fig. 8G). These three maps are directly comparable to the anterior ~60% of the map of the *WT* tongue shown in Fig. 1B. In each *Celsr1*$^{-/-}$ tongue, two narrow stripes located along the sides of the anterior region at a distance of 1–1.5 mm from the midline contain large numbers of LP that are misoriented by ~180 degrees, i.e. they point from posterior-to-anterior instead of anterior-to-posterior. Adjacent to these stripes, many LP are oriented in a manner that minimizes local differences in LP orientation, producing a gradual transition of orientations over a 180-degree range. The stereotypy in the *Celsr1*$^{-/-}$ LP vector maps is reminiscent of the stereotyped patterns of wing hair misorientation in PCP mutant *Drosophila* (Adler et al., 1987). In both

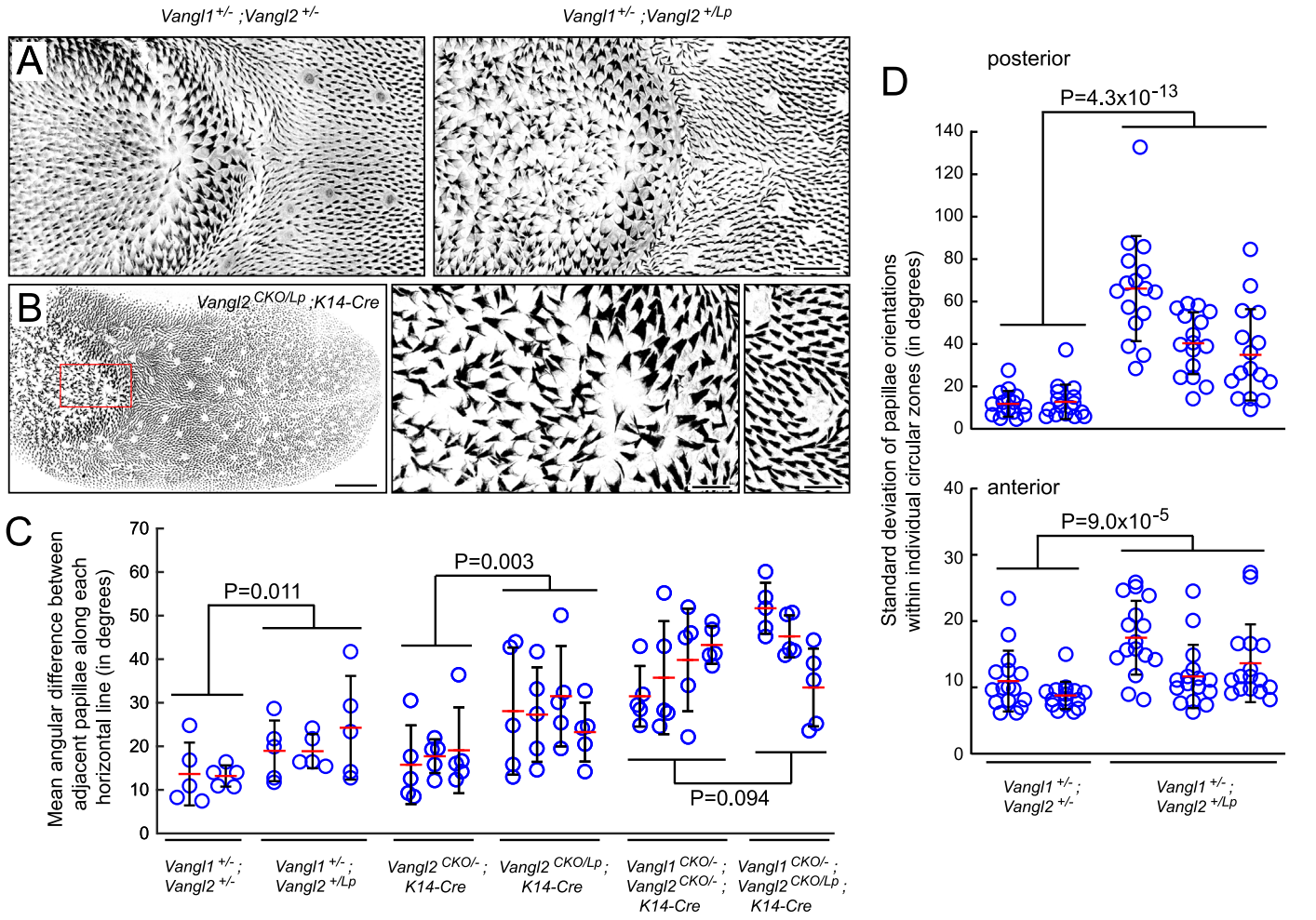

Fig. 7. Quantitative comparison of LP misorientation produced by *Vangl2*^{KO} vs. *Vangl2*^{Lp} alleles. (A) The posterior ~40% of the dorsal surface of *Vangl1*$^{+/-}$;*Vangl2*$^{+/-}$ and *Vangl1*$^{+/-}$;*Vangl2*$^{+/Lp}$ tongues at P30. (B) P30 *Vangl2*$^{CKO/Lp}$;*K14-Cre* tongue (left), flower region (center), and anterior region (right) displayed as in Fig. 2. (C) Three pairs of comparisons of local LP orientation for P30 tongues using the line method. Each set of five data points are derived from one tongue of the indicated genotype. Pairwise comparisons are between genotypes differing only by the replacement of a *Vangl2* null allele for a *Vangl2*^{Lp} allele. P-values are indicated for each pairwise comparison. (D) Comparison between posterior (top) and anterior (bottom) territories of *Vangl1*$^{+/-}$;*Vangl2*$^{+/-}$ and *Vangl1*$^{+/-}$;*Vangl2*$^{+/Lp}$ tongues using the circle method, as shown in Fig. 5. Scale bars: (A), 400 μm; (B), 1 mm (left), 200 μm (center and right).

systems, other morphogenetic signals or anatomic structures, such as fungiform papillae or wing veins, may constrain the patterns that can emerge in the mutant epithelium.

To quantify the global LP misorientation phenotype in *Celsr1*$^{-/-}$ tongues, we employed a third quantification method – referred to as the "grid method" – in which 216 0.25 mm × 0.25 mm squares, arranged into a 12 × 18 rectangle, were overlaid on the anterior region and the average orientation of the ~10 LP within each grid square was estimated by visual inspection (Fig. 9A). The bar graphs in Fig. 9B and C show the orientations of the 216 vectors, plotted separately for the left and right sides of the tongue for the same three *Celsr1*$^{-/-}$ tongues that were used to create the vector maps in Fig. 8G, as well as the same eight tongues from the *Vangl1;Vangl2;Nkx2.5-Cre* series analyzed in Figs. 5 and 6. Not surprisingly, inactivation of greater numbers of *Vangl* genes leads to a broadening of the angular distribution of the averaged LP vectors (Fig. 9C). However, even with all four *Vangl* genes deleted (*Vangl1*$^{CKO/-}$;*Vangl2*$^{CKO/-}$;*Nkx2.5-Cre*) nearly all of the averaged LP vectors point in the anterior-to-posterior direction, represented by angles between 90 and 270 degrees in Fig. 9C. By contrast, in *Celsr1*$^{-/-}$ tongues, approximately half of the average LP vectors point in the posterior-to-anterior direction, represented by angles between 0 and 90 degrees and 270 and 360 degrees in Fig. 9B.

These data demonstrate that the *Celsr1*$^{-/-}$ phenotype is qualitatively and quantitatively distinct from the phenotypes associated with the conditional *Vangl* series. A potential explanation for these differences is that *Celsr1* may function in signaling systems for both local and global orientation, whereas *Vangl* family members may function only or predominantly in a signaling system for local orientation. An alternate explanation is that these differences might reflect the constitutive nature of the *Celsr1* null alleles in contrast to the in utero elimination of conditional *Vangl* function by *K14-Cre* and *Nkx2.5-Cre*. This alternate explanation implies that *Vangl* expression in the tongue primordium prior to Cre-mediated recombination and/or the persistence of small amounts of *Vangl* protein after Cre-mediated recombination might promote global signals for LP orientation that are missing in the *Celsr1*$^{-/-}$ tongue.

3. Discussion

3.1. The tongue epithelium as a system for quantitative analysis of PCP

The experiments reported here establish the mouse tongue as a favorable system for studying PCP control of epithelial patterning. Phenotyping is based on a simple flat mount preparation that

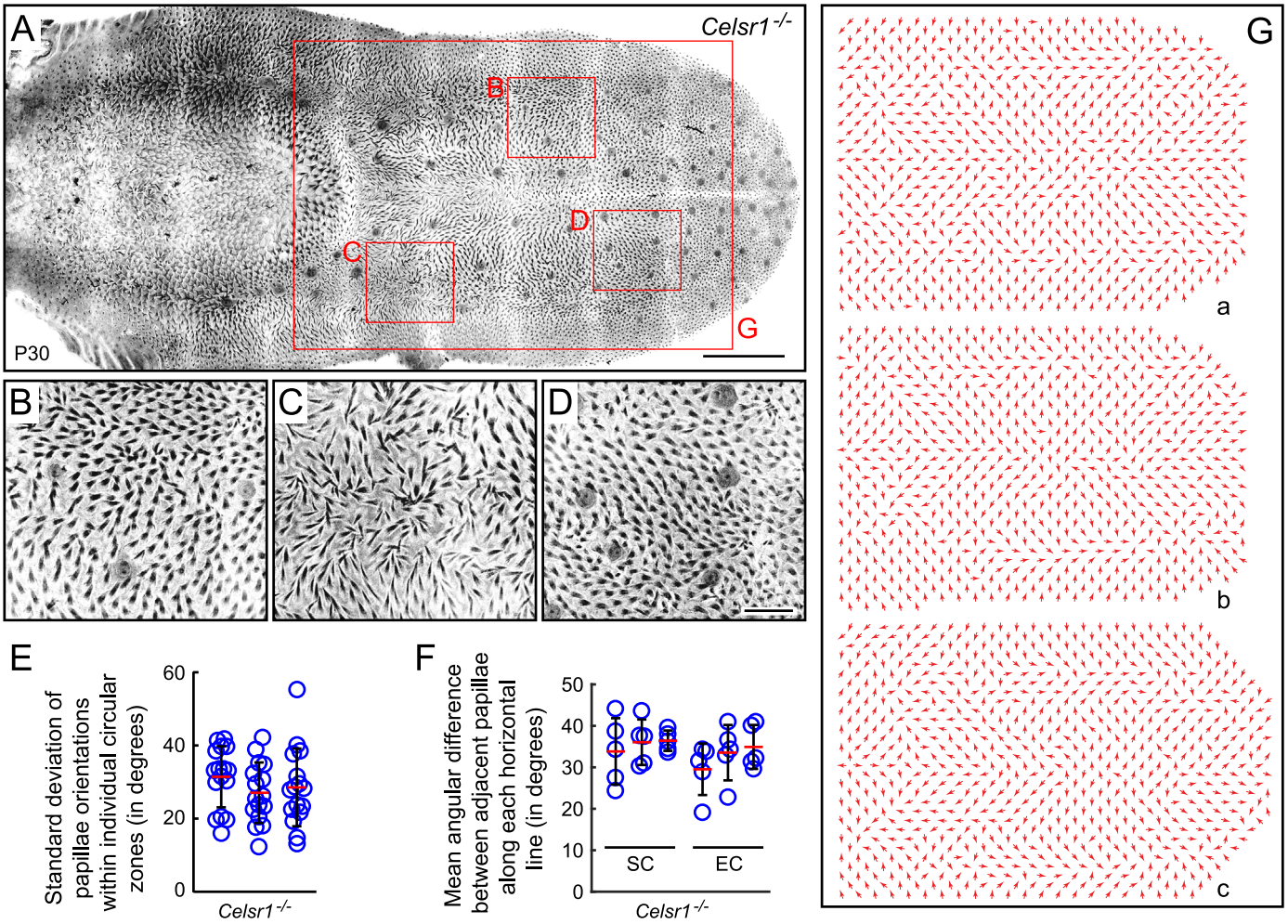

Fig. 8. *Celsr1*$^{-/-}$ LP exhibit defects in both local and global orientation. (A–D) Stitched tongue image of a *Celsr1*$^{-/-}$ tongue at P30 (A) with three regions enlarged (B–D). (E,F) The circle (E) and line (F) methods of quantifying local orientation of LP for three P30 *Celsr1*$^{-/-}$ tongues. In (F), line method quantifications compared the standard counting method (SC, each scored papilla overlaps the horizontal scoring line) to an extended counting method (EC, a circular territory centered on each papillae overlaps the horizontal scoring line), as illustrated in Fig. 6C. (G) Manual scoring of the LP vector field for the same three P30 *Celsr1*$^{-/-}$ tongues analyzed in (E) and (F), as in Fig. 1B, except the region scored in (G) is confined to the territory anterior to the center of the flower region as demarcated by the large red rectangle in (A). Scale bars: (A), 1 mm; (B–D), 200 μm.

facilitates quantitative analyses of the LP that cover the dorsal surface. In *WT* mice, the LP pattern is highly stereotyped, so that any small deviations in global or local features are readily apparent. Taking advantage of data sets that can be represented as two dimensional vector fields, we have developed and applied three procedures for quantifying LP orientations – the circle, line, and grid methods – and we have used them to assess deviations from *WT*. In particular, we have used these methods to define the phenotypes generated by partial or complete inactivation of *Vangl1* and *Vangl2* and by inactivation of *Celsr1*, and made the unexpected observation that inactivation of *Vangl* function starting at ~E12 predominantly or exclusively alters LP orientation in a local manner, whereas constitutive inactivation of *Celsr1* produces both global and local orientation defects. These gene mutations do not alter the division of the tongue surface into flower and anterior regions, implying that an independent – and, as yet, undetermined – signaling system is responsible for these global patterning features.

The quantitative analyses developed here use information from only a small fraction of the ~7000 LP on the surface of the mouse tongue. This sampling strategy was necessitated by our reliance on manual scoring of LP orientations, an approach that is easy to implement but tedious to perform. Looking ahead, we can envision various ways in which additional information can be extracted from tongue flat mount images. For example, it may be possible to use machine vision to automatically identify the locations and orientations of each LP. The challenge for this approach is to develop algorithms that can recognize diverse LP morphologies and correctly segment overlapping LP. With respect to LP recognition, the highly stereotyped variation in LP morphology in different tongue locations should permit the use of X-Y location within an image to refine the parameters for LP recognition. More precise comparisons between different tongue images, including the definition of a standard X-Y template, will require local warping and alignment of images that differ due to biological variation and the effects of sample preparation. Algorithms that warp and align images to match a template have been developed for brain histology and magnetic resonance imaging (Avants et al., 2014; Economo et al., 2016) and might be adaptable to tongue images. If these technical challenges can be met, it should be possible to generate LP vector maps at single LP resolution and to compare WT and mutant maps to reveal the magnitude and statistical significance of variation in LP orientation at every X-Y location.

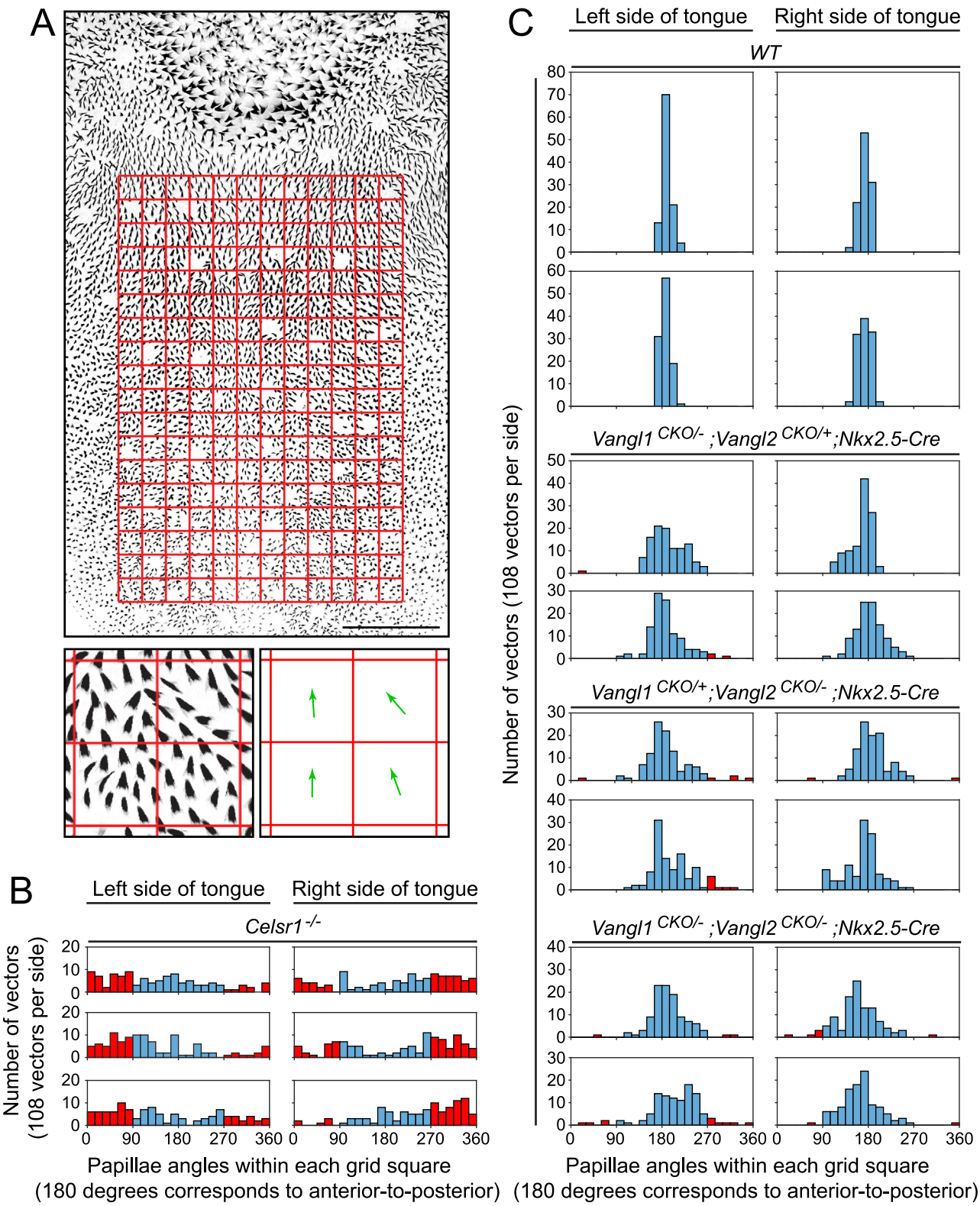

Fig. 9. Quantitative comparisons of global orientation of LP in the anterior tongue region for *WT*, *Celsr1*$^{-/-}$, and *Vangl1/Vangl2* conditional mutant combinations. (A) The standard placement of a grid of 12 × 18 squares (each 0.25 × 0.25 mm) within the anterior region (upper) and manual scoring of mean LP orientation for the ~12 LP within each square by a single arrow (lower). (B,C) Angular distribution of the grid method orientation vectors for *Celsr1*$^{-/-}$ (B) and *WT* and *Vangl1/Vangl2* series tongues (C). The 108 vectors from the left and right sides of each tongue have been plotted separately. Vectors within 90 degrees of the anterior-to-posterior axis are plotted as blue bars; vectors more than 90 degrees from the anterior-to-posterior axis (i.e. pointed toward the anterior more than the posterior) are plotted as red bars. Scale bar in (A): 1 mm.

3.2. Comparisons between lingual papillae and hair follicles

It is interesting to compare the patterning of hair follicles and LP and the effects of PCP gene mutations on these two epidermal derivatives (Wang et al., 2006a; Hua et al., 2014; Chang et al., 2016; this work). On hair-covered regions of skin and on the dorsal surface of the tongue, WT mice develop stereotyped patterns of hair follicles and LP that show a high degree of order on both local

and global scales. For hair follicles, global order on the head and back is seen in the anterior-to-posterior orientations of follicles, and on the limbs and feet it is seen in the proximal-to-distal orientations of follicles. For LP, global order is seen in the anterior-to-posterior orientation of LP anteriorly and in the flower pattern posteriorly. Local order minimizes differences in the orientations of neighboring hair follicles and neighboring LP.

For hair follicles, the PCP phenotype is most apparent early in development, when it leads to an approximate randomization of orientations among immature follicles. As development proceeds, hair follicles reorient in a PCP-independent refinement process that minimizes angular differences between neighbors, simultaneously increasing local order and creating large-scale patterns that appear to arise from random variation in orientations within the immature field of follicles (Wang et al., 2010). From our analysis of PCP phenotypes in P30 tongues, the degree of local order among LP appears to be lower than that observed among PCP mutant hair follicles after the first postnatal week, as seen, for example, in Fig. 6 of Wang et al. (2010). We can rationalize the greater degree of local disorder in the LP system relative to the hair follicle system by supposing that, if the tongue has an analogue of the PCP-independent refinement process, then its strength or duration of action may be reduced relative to the refinement process for hair follicles.

The most obvious anatomic difference between hair follicles and LP is that follicles are formed by invaginations into the dermis, whereas LP consist of protrusions above the plane of the tongue surface. In the case of hair follicles, one can readily envision mechanical signaling between adjacent follicles via tension or compression within the surrounding dermis or chemical signaling between adjacent follicles via diffusion of signaling molecules through the dermis. One or both types of communication presumably account for the reorienting movements that locally align follicles in both WT and PCP mutant skin. In the tongue, communication of polarity information likely occurs during embryonic development prior to the protrusion of LP cells above the tongue surface. Whether LP orientations can be modified after the time when LP protrude from the tongue surface is an open question.

Defects in PCP appear to have no effect on the intrinsic structure, location, or density of hair follicles or of LP. Instead, the PCP phenotype is limited to defects in the orientations of these structures within the plane of the epithelium. Since hair follicles and LP are both multicellular epithelial structures, acquiring a particular orientation requires coordinated multicellular behavior. Thus, hair follicle and LP orientation likely involve cellular mechanisms in addition to those required for the orientation of individual epithelial cells within a monolayer.

3.3. A hierarchy of patterning systems

The presence of macroscopic patterning features, such as the flower region, and microscopic patterning features, such as the region-specific sizes and shapes of LP, suggests the existence of a hierarchy of patterning systems, each devoted to a particular feature of epithelial patterning on the tongue surface. In this conceptual hierarchy, PCP occupies a middle ground, controlling the orientations of the elementary building blocks of the pattern. The different degrees of LP misorientation at different tongue locations in PCP mutants imply an interaction between local and global patterning systems. The presence of defects in both local and global orientation in *Celsr1*$^{-/-}$ tongues additionally suggests a mechanistic connection between these systems.

4. Materials and methods

4.1. Mouse lines and antibodies

The following mouse alleles were used: *Celsr1*^{KO} (Qu et al., 2010), *Hprt-LSL-tdT* (Wu et al., 2014), *K17-GFP* (Bianchi et al., 2005; a kind gift of Dr. Pierre Coulombe, Johns Hopkins University), *K14-Cre* (Dassule et al., 2000; JAX 004782), *Nkx2.5-Cre* (Moses et al., 2001; a kind gift of Dr. Robert Schwartz, University of Houston), *Prickle2*^{KO} (Tao et al., 2011), *Vangl2*^{CKO} (Copley et al., 2013), *Vangl2*^{Lp} (Strong and Hollander, 1949; a kind gift of Dr. Xiaowei Lu, University of Virginia), and *Vangl* ^{KO} (Chang et al., 2016). In the text and figure legends, when genotypes lacking *Cre* are presented, *CKO* alleles are represented by +. Table S2 lists the genotypes studied. Mice were handled and housed according to the approved Institutional Animal Care and Use Committee (IACUC) protocol MO13M469 of the Johns Hopkins Medical Institutions.

4.2. Tissue preparation for light and electron microscopy

For tongue flat mounts, mice were sacrificed at P30 and the lower jaw with the attached tongue was removed and fixed in 1% PFA in phosphate buffered saline (PBS) at room temperature for 2 h. The tongues were removed from the lower jaws and then fixed in 1% PFA at 4 °C overnight, dorsal side down while being pressed with a circular mesh insert (Netwell 12 Well Insert, 74 μm mesh; Corning EK-680210) against the bottom of the well of a 6-well plate. Since the Netwell insert protrudes above the top of the well, pressure on the tongue was maintained by gentle pressure on the cover of the 6-well plate. The next day, the fixed and flattened tongues were washed in PBS, and the ventral ~75% of the tongue was trimmed away with iris scissors, leaving a 0.5–1 mm thick layer of tissue adjacent to the dorsal surface, which was mounted dorsal-side up in Flouromount-G (Southern Biotech 0100-01). For tissue sections, embryos were immersion fixed in 1% PFA at 4 °C for 16 h, embedded in 3% SeaPlaque Agarose (Lonza 50100), and sectioned at 200 μm thickness with a Leica VT1200 vibratome.

For scanning electron microscopy, tongues were immersion fixed in 4% paraformaldehyde in phosphate buffered saline with 1 mM $MgCl_2$ and 1 mM $CaCl_2$ (PBSMC) overnight at 4 °C, and then fixed for an additional 24 h in 2% paraformaldehyde, 2% gluteraldehyde in PBSMC at 4 °C. After three 15 min room temperature washes in 0.1 M sodium cacodylate, the tongues were fixed in 1% osmium tetroxide, 0.1 M sodium cacodylate for one hour on ice in the dark, then washed twice in water, dehydrated through a graded ethanol series, and washed for five minutes in 1:1 ethanol: hexamethyldisilazane (HMDS), followed by two five-minute washes in HMDS before overnight dessication. The dessicated tongues were sputter-coated with gold-palladium to a thickness of 20–30 nm and imaged with a LEO 1530 field emission scanning electron microscope.

4.3. Confocal microscopy

Whole-mount and sectioned tongues were scanned with a Zeiss LSM700 confocal microscope at 10 ×, zoom 0.5, with 10–20 Z-planes spaced 5 μm apart, and with 10% overlap between adjacent tiles. The images were stitched together and projected along the Z-axis using Zen software (Zeiss).

4.4. Image analysis

Whole tongue images were inverted and contrast-enhanced in Adobe Photoshop. LP orientations were scored manually using ImageJ. Subsequent analyses were performed in Excel (Microsoft)

and R. > 19,000 LP orientations were scored. Standard deviation and P-values were calculated using R. For the circle method, the circular standard deviation [the square root of $2(1-r)$, where r is the mean vector length for the sample; Zar, 1999] was calculated using R.

Acknowledgements

The authors thank Tyler Stevens for assistance with scanning electron microscopy, Robert Schwartz and Xiaowei Lu for mice, and Hao Chang and Mark Sabbagh for helpful comments on the manuscript. Supported by the Howard Hughes Medical Institute, United States, (YW, JW, and JN), the National Eye Institute (NIH), United States, 1R01EY018637 (AR), the National Institute of Neurologic Disease and Stroke (NIH), United States, 1R01NS098590-01 (SW and AGB), and Actions de Recherches Concertées (ARC-10/15-026), PDR-FNRS T0002.13, Interuniversity Poles of Attraction (SSTC, PAI7/20), and WELBIO-CR-2012A-07 from Région Wallonne (AMG), Belgium.

Appendix A. Supporting information

Supplementary data associated with this article can be found in the online version at http://dx.doi.org/10.1016/j.ydbio.2016.09.004.

References

Adler, P.N., 2002. Planar signaling and morphogenesis in Drosophila. Dev. Cell 2, 525–535.
Adler, P.N., Charlton, J., Vinson, C., 1987. Allelic variation at the frizzled locus of Drosophila. Dev. Genet. 8, 99–119.
Avants, B.B., Tustison, N.J., Stauffer, M., Song, G., Wu, B., Gee, J.C., 2014. The Insight ToolKit image registration framework. Front. Neuroinform. 8, 44.
Bianchi, N., Depianto, D., McGowan, K., Gu, C., Coulombe, P., 2005. Exploiting the keratin 17 gene promoter to visualize live cells in epithelial appendages of mice. Mol. Cell. Biol. 25, 7249–7259.
Bininda-Emonds, O.R., Cardillo, M., Jones, K.E., MacPhee, R.D., Beck, R.M., Grenyer, R., Price, S.A., Vos, R.A., Gittleman, J.L., Purvis, A., 2007. The delayed rise of present-day mammals. Nature 446, 507–512.
Boutin, C., Labedan, P., Dimidschstein, J., Richard, F., Cremer, H., André, P., Yang, Y., Montcouquiol, M., Goffinet, A.M., Tissir, F., 2014. A dual role for planar cell polarity genes in ciliated cells. Proc. Natl. Acad. Sci. USA 111, E3129–E3138.
Chang, H., Smallwood, P.M., Williams, J., Nathans, J., 2016. The spatio-temporal domains of Frizzled6 action in planar polarity control of hair follicle orientation. Dev. Biol. 409, 181–193.
Copley, C.O., Duncan, J.S., Liu, C., Cheng, H., Deans, M.R., 2013. Postnatal refinement of auditory hair cell planar polarity deficits occurs in the absence of Vangl2. J. Neurosci. 33, 14001–14016.
Curtin, J.A., Quint, E., Tsipouri, V., Arkell, R.M., Cattanach, B., Copp, A.J., Henderson, D.J., Spurr, N., Stanier, P., Fisher, E.M., Nolan, P.M., Steel, K.P., Brown, S.D., Gray, I. C., Murdoch, J.N., 2003. Mutation of Celsr1 disrupts planar polarity of inner ear hair cells and causes severe neural tube defects in the mouse. Curr. Biol. 13, 1129–1133.
Dassule, H.R., Lewis, P., Bei, M., Maas, R., McMahon, A.P., 2000. Sonic hedgehog regulates growth and morphogenesis of the tooth. Development 127, 4775–4785.
Deans, M.R., Antic, D., Suyama, K., Scott, M.P., Axelrod, J.D., Goodrich, L.V., 2007. Asymmetric distribution of prickle-like 2 reveals an early underlying polarization of vestibular sensory epithelia in the inner ear. J. Neurosci. 27, 3139–3147.
Devenport, D., Fuchs, E., 2008. Planar polarization in embryonic epidermis orchestrates global asymmetric morphogenesis of hair follicles. Nat. Cell Biol. 10, 1257–1268.
Doran, G.A., 1975. Review of the evolution and phylogeny of the mammalian tongue. Acta Anat. 91, 118–129.
Economo, M.N., Clack, N.G., Lavis, L.D., Gerfen, C.R., Svoboda, K., Myers, E.W., Chandrashekar, J., 2016. A platform for brain-wide imaging and reconstruction of individual neurons. Elife 5, e10566.
Goodrich, L.V., Strutt, D., 2011. Principles of planar polarity in animal development. Development 128, 1877–1892.
Guo, N., Hawkins, C., Nathans, J., 2004. Frizzled6 controls hair patterning in mice. Proc. Natl. Acad. Sci. USA 101, 9277–9281.
Hua, Z.L., Chang, H., Wang, Y., Smallwood, P.M., Nathans, J., 2014. Partial interchangeability of Fz3 and Fz6 in tissue polarity signaling for epithelial orientation and axon growth and guidance. Development 141, 3944–3954.
Iwasaki, S., 2002. Evolution of the structure and function of the vertebrate tongue. J. Anat. 201, 1–13.
Kutuzov, H., Sicher, H., 1951. The filiform and conical papillae of the tongue in the white rat. Anat. Rec. 110, 275–288.
Kutuzov, H., Sicher, H., 1953. Comparative anatomy of the mucosa of the tongue and the palate of the laboratory mouse. Anat. Rec. 116, 409–425.
Lawrence, P.A., Struhl, G., Casal, J., 2007. Planar cell polarity: one or two pathways? Nat. Rev. Genet. 8, 555–563.
Matis, M., Axelrod, J.D., 2013. Regulation of PCP by the Fat signaling pathway. Genes Dev. 27, 2207–2220.
Montcouquiol, M., Rachel, R.A., Lanford, P.J., Copeland, N.G., Jenkins, N.A., Kelley, M. W., 2003. Identification of Vangl2 and Scrb1 as planar polarity genes in mammals. Nature 423, 173–177.
Moses, K.A., DeMayo, F., Braun, R.M., Reecy, J.L., Schwartz, R.J., 2001. Embryonic expression of an Nkx2-5/Cre gene using ROSA26 reporter mice. Genesis 31, 176–180.
Murdoch, J.N., Doudney, K., Paternotte, C., Copp, A.J., Stanier, P., 2001. Severe neural tube defects in the loop-tail mouse result from mutation of Lpp1, a novel gene involved in floor plate specification. Hum. Mol. Genet. 10, 2593–2601.
Ohata, S., Nakatani, J., Herranz-Pérez, V., Cheng, J., Belinson, H., Inubushi, T., Snider, W.D., García-Verdugo, J.M., Wynshaw-Boris, A., Alvarez-Buylla, A., 2014. Inactivation of Dishevelleds disrupts planar polarity in ependymal motile cilia and results in hydrocephalus. Neuron 83, 558–571.
Qu, Y., Glasco, D.M., Zhou, L., Sawant, A., Ravni, A., Fritzsch, B., Damrau, C., Murdoch, J.N., Evans, S., Pfaff, S.L., Formstone, C., Goffinet, A.M., Chandrasekhar, A., Tissir, F., 2010. Atypical cadherins Celsr1-3 differentially regulate migration of facial branchiomotor neurons in mice. J. Neurosci. 30, 9392–9401.
Ravni, A., Qu, Y., Goffinet, A.M., Tissir, F., 2009. Planar cell polarity cadherin Celsr1 regulates skin patterning in the mouse. J. Invest. Dermatol. 129, 2507–2509.
Sharp, K.A., Axelrod, J.D., 2016. Prickle isoforms control the direction of tissue polarity by microtubule independent and dependent mechanisms. Biol. Open 5, 229–236.
Shi, D., Komatsu, K., Hirao, M., Toyooka, Y., Koyama, H., Tissir, F., Goffinet, A.M., Uemura, T., Fujimori, T., 2014. Celsr1 is required for the generation of polarity at multiple levels of the mouse oviduct. Development 141, 4558–4568.
Strong, L.C., Hollander, W.F., 1949. Hereditary loop-tail in the house mouse accompanied by imperforate vagina and with lethal craniorachischisis when homozygous. J. Hered. 40, 329–334.
Tao, H., Manak, J.R., Sowers, L., Mei, X., Kiyonari, H., Abe, T., Dahdaleh, N.S., Yang, T., Wu, S., Chen, S., Fox, M.H., Gurnett, C., Montine, T., Bird, T., Shaffer, L.G., Rosenfeld, J.A., McConnell, J., Madan-Khetarpal, S., Berry-Kravis, E., Griesbach, H., Saneto, R.P., Scott, M.P., Antic, D., Reed, J., Boland, R., Ehaideb, S.N., El-Shanti, H., Mahajan, V.B., Ferguson, P.J., Axelrod, J.D., Lehesjoki, A.E., Fritzsch, B., Slusarski, D.C., Wemmie, J., Ueno, N., Bassuk, A.G., 2011. Mutations in prickle orthologs cause seizures in flies, mice, and humans. Am. J. Hum. Genet. 88, 138–149.
Tissir, F., Qu, Y., Montcouquiol, M., Zhou, L., Komatsu, K., Shi, D., Fujimori, T., Labeau, J., Tyteca, D., Courtoy, P., Poumay, Y., Uemura, T., Goffinet, A.M., 2010. Lack of cadherins Celsr2 and Celsr3 impairs ependymal ciliogenesis, leading to fatal hydrocephalus. Nat. Neurosci. 13, 700–707.
Torban, E., Patenaude, A.M., Leclerc, S., Rakowiecki, S., Gauthier, S., Andelfinger, G., Epstein, D.J., Gros, P., 2008. Genetic interaction between members of the Vangl family causes neural tube defects in mice. Proc. Natl. Acad. Sci. USA 105, 3449–3454.
Vladar, E.K., Bayly, R.D., Sangoram, A.M., Scott, M.P., Axelrod, J.D., 2012. Microtubules enable the planar cell polarity of airway cilia. Curr. Biol. 22, 2203–2212.
Wang, J., Mark, S., Zhang, X., Qian, D., Yoo, S.J., Radde-Gallwitz, K., Zhang, Y., Lin, X., Collazo, A., Wynshaw-Boris, A., Chen, P., 2005. Regulation of polarized extension and planar cell polarity in the cochlea by the vertebrate PCP pathway. Nat. Genet. 37, 980–985.
Wang, Y., Badea, T., Nathans, J., 2006a. Order from disorder: self-organization in mammalian hair patterning. Proc. Natl. Acad. Sci. USA 103, 19800–19805.
Wang, Y., Guo, N., Nathans, J., 2006b. The role of Frizzled3 and Frizzled6 in neural tube closure and in the planar polarity of inner-ear sensory hair cells. J. Neurosci. 26, 2147–2156.
Wang, Y., Chang, H., Nathans, J., 2010. When whorls collide: the development of hair patterns in frizzled 6 mutant mice. Development 137, 4091–4099.
Wu, H., Luo, J., Yu, H., Rattner, A., Mo, A., Wang, Y., Smallwood, P.M., Erlanger, B., Wheelan, S.J., Nathans, J., 2014. Cellular resolution maps of X chromosome inactivation: implications for neural development, function, and disease. Neuron 81, 103–119.
Yin, H., Copley, C.O., Goodrich, L.V., Deans, M.R., 2012. Comparison of phenotypes between different vangl2 mutants demonstrates dominant effects of the Looptail mutation during hair cell development. PLoS One 7, e31988.
Zar, J.H., 1999. Biostatistical Analysis, 4th ed Prentice Hall, Upper Saddle River, New Jersey, USA.